atmosphere

MDPI

Article

Analysis of Intraseasonal Oscillation Features of Winter Cold Precipitation Events in Southern China

Qingjiu Gao *, Ziqi Zhang, Yesheng Zhu and Shuyi Chen

Key Laboratory of Meteorological Disaster of Ministry of Education (KLME), Joint International Research Laboratory of Climate and Environment Change (ILCEC), Collaborative Innovation Center on Forecast and Evaluation of Meteorological Disasters (CIC-FEMD), Nanjing University of Information Science & Technology, Nanjing 210044, China

* Correspondence: gaoqj@nuist.edu.cn

Abstract: Based on the daily minimum air temperature (T_{min}) data and the daily precipitation data from the NCC/CMA combined with the NCEP/DOE reanalysis data, the intraseasonal features and circulations of the winter cold precipitation events (CPEs) in southern China under the influence of strong Madden–Julian oscillation (MJO) were explored. The results show that: (1) Winter temperatures in southern China are characterized by intraseasonal oscillations (ISOs) of 10–30-d and 30–60-d, with six CPEs under strong MJO all occurring during these two intraseasonal scales in cooling phases. The invasion of cold air coupled with the availability of appropriate moisture conditions in southern China is more conducive to the CPEs. (2) A cyclone and anticyclone lying to the east of the Ural Mountains and the northwest of Lake Baikal at 925-hPa gradually move southeastward. The merging of the low-frequency (LF) blocking highs over the Ural Mountains and the North Pacific Ocean at 500-hPa leads to the contraction and southward movement of the LF cold vortex. The following anomalous northerly winds steer the cold air towards southern China. The cold advection is the dominant term in the cooling process, while the adiabatic cooling accompanied with ascending motion is also beneficial to the cooling process. (3) MJO has some effect on the LF blocking highs and the cold vortex in the mid-high latitudes and induces the CPEs over southern China. The joint effect of mid-high and low latitudes on the 30–60-d intraseasonal oscillation scale can have a significant impact on the cooling and precipitation processes of CPEs.

Keywords: low frequency; MJO; cold precipitation events; southern China

Citation: Gao, Q.; Zhang, Z.; Zhu, Y.; Chen, S. Analysis of Intraseasonal Oscillation Features of Winter Cold Precipitation Events in Southern China. *Atmosphere* **2022**, *13*, 1603. https://doi.org/10.3390/atmos13101603

Academic Editor: Eduardo García-Ortega

Received: 27 August 2022
Accepted: 26 September 2022
Published: 30 September 2022

1. Introduction

Recent evidence suggests that extreme weather events have been occurring against the background of global warming, with an increasing trend in the intensity as well as the duration of extreme low-temperature events in winter since the late 1990s [1–4]. For instance, two record-breaking low-temperature events occurred in the winter of 2020/2021 in China, with the temperatures in Beijing and Tianjin reaching the lowest in the past 54 years [5]. As an economically developed and populous region, southern China is subject to different timescale circulations in the East Asian winter monsoon, with extremely low temperatures, rain, and snow frequently in winter, causing great losses in the national economy and people's everyday lives [6–10]. Thus, extreme low-temperature events have been attracting a lot of interest.

The intraseasonal oscillation (ISO) is closely associated with weather and climate conditions. It was first discovered by Madden and Julian in the early 1970s. They revealed [11,12] that the tropical atmospheric pressure and latitudinal wind fields oscillated with a period of 40–50-d. This eastward propagating fluctuation is usually called Madden–Julian oscillation (MJO). Anderson and Rosen [13] have further demonstrated that the ISO exists not only in the tropical atmosphere but also in the mid-high latitudes. Extensive research on ISO

has been performed by many scholars [14–16]. The results have pointed out that ISO exists all over the world, even in the Tibetan Plateau and the stratosphere [17–20]. ISO plays a vital role in the evolution of the climate and has a significant impact on the development of persistent extreme weather events [21–24].

Researchers have found that the feature of ISO over the Eurasian mid-high latitude in boreal winter is a common condition which has a considerable impact on winter extreme cold events in China [25–28]. For example, Zhu and Jiang [29] showed the remote correlation between active tropical convection over the Indian Ocean and the strengthening of the low-frequency (LF) Siberia high. It was shown that the integrated effect of ISOs over mid-high latitudes and low latitude plays a critical role in the development of persistent cold events in China during winter. Miao et al. [30] revealed that the LF wave train at the 500-hPa level propagating along the Ural Mountains–Lake Baikal at mid-high latitudes in the Northern Hemisphere was the key circulation system responsible for a cold event in northeastern China. Yu and Gao [31] found that 10–20-d LF northerly winds guide the advance of cold air southward at high latitudes, thus causing a severe extreme cold event in the southern region in 1996. Jiang and Yao [32] analyzed and found that a cold center with quasi-biweekly oscillations had a major influence on the cold event in southern China in January 2016. However, these studies were based on individual cases, thus raising the question regarding the key LF circulation anomalies mentioned above. Therefore, it is necessary to provide a comprehensive study of more winter cold events.

MJO can also have an impact on winter low temperatures and precipitation. Convective heating anomalies caused by the MJO have been demonstrated to stimulate the northward Rossby wave train, which affects the circulation of mid-high latitudes in a teleconnection, thereby enhancing cold air activity and resulting in extensive rain and snow in China [33,34]. For example, the "historic" southern low temperatures and heavy precipitation events in 2008 [35] and the persistent snow in northern China in November 2009 [36] were related to the strong convective activity of the MJO.

In an attempt to provide some basis for forecasting cold precipitation events (CPEs) in the winter, as well as defending against and mitigating the disasters caused by CPEs, we explored the mechanism of the six CPEs that occurred concurrently during the winter of 1979–2019 in southern China under the influence of strong MJO. This paper is organized as follows: Section 2 introduces the data and methods used in this paper and the definition of CPEs in the context of a strong MJO. Section 3 reveals the characteristics of the winter-temperature ISO in the southern region, and the LF precipitation and temperature during the CPEs are discussed. Section 4 analyzes and diagnoses the ISO characteristics and the evolution of the circulations during the CPEs. Section 5 explores the effect of MJO on CPEs, and the final section concludes the paper with a summary and discussion.

2. Data and Methods

2.1. Data

The daily minimum temperature (T_{min}) recorded at 2472 stations in China from gauge observations was obtained from China's Ground Temperature Gridded Dataset (Version 2.0) with a horizonal resolution of 0.5° × 0.5°, provided by the National Climate Center of China Meteorological Administration (NCC/CMA).

The precipitation data [37] were based on the China regional grid precipitation dataset CN05.1 of the China Meteorological Data Network, constructed by the thin-plate spline (TPS) and angular distance weighting (ADW) method during the interpolation with more than 2400 station observations in China.

The reanalysis data used in this study were of several meteorological fields including the daily geopotential height, temperature, wind, and vertical velocity from the National Centers for the Environment/Department of Energy (NCEP/DOE), with a horizontal resolution of 2.5° × 2.5° from 1000–10-hPa levels, as well as the daily specific humidity with 8 vertical pressure levels (1000–300-hPa). Daily outgoing longwave radiation (OLR) data [38], with a horizontal resolution of 2.5° × 2.5° and produced by the National Oceanic

and Atmospheric Administration's (NOAA) polar-orbiting satellites, were utilized to represent tropical convections. The daily RMM index defined by Wheeler and Hendon [39] can be downloaded from the Bureau of Meteorology of Australia (http://www.bom.gov.au/climate/mjo/graphics/rmm.74toRealtime.txt, accessed on 15 January 2022).

The period of the data spanned from 1 January 1979 to 31 December 2019. It should be noted that this paper takes December of one year to February of the following year as the winter of that year, e.g., the winter of 1979 means December 1979–February 1980.

2.2. The Definition of Thresholds, Cold Precipitation Events, and Strong MJO

Referring to the method of Peng and Bueh [40], for a calendar day, the percentile was calculated from five-day windows centered on that calendar day for all years. Therefore, the 15th percentile threshold for each calendar day was determined from an ascending order of 205 days (41 years $*$ 5 days). This was used to obtain the extreme low-temperature daily threshold for 365 days (29 February was removed). The average daily thresholds for December, January, and February were taken as the thresholds for the cold events in this paper (Figure 1). It can be seen that the thresholds varied between 0 and -5 °C in the middle–lower reaches of the Yangtze River and Jiangnan, 0 and 5 °C in the northern region of South China, the Sichuan Basin, and Southwest China, and around 5~10 °C in the southern region of South China, which is a more stringent threshold criterion to identify southern cold events.

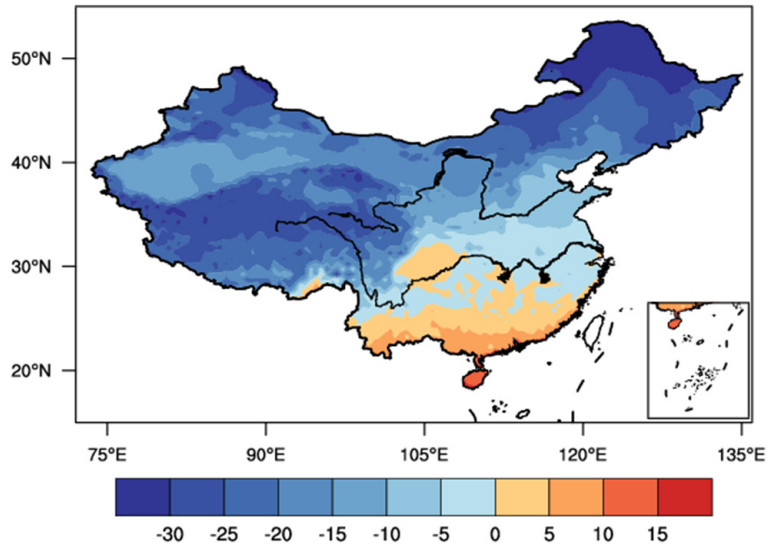

Figure 1. Average daily thresholds for extreme low temperatures (units: °C) in winter from 1979 to 2019 in China.

The area average of the difference between the T_{min} and the threshold at each grid point for southern China (20°–30° N, 105°−122.5° E) was computed. When this difference was less than or equal to zero, the day was described as a cold day. If the cold day reached six consecutive days or more (one intermittent day was permitted), it was recorded as an extreme cold event in southern China. The cold event with the maximum amplitude and both the minimum amplitudes exceeding ±0.5 standard deviation in the time series of the area-averaged band-pass filtered T_{min} minus threshold was characterized as a cold event related to the intraseasonal oscillation. Combined with the daily precipitation data, a cold precipitation event (CPE) was referred to as precipitation in the southern region during the cold event.

Considering the influence of the MJO, the RMM index was used to classify a strong MJO event. If the number of days with $RMM1^2 + RMM2^2 < 1$ did not exceed 3 days, it was defined as a strong MJO event. Finally, we selected 6 CPEs with a strong MJO background. The MJO activity track during the CPEs are shown in Figure 2.

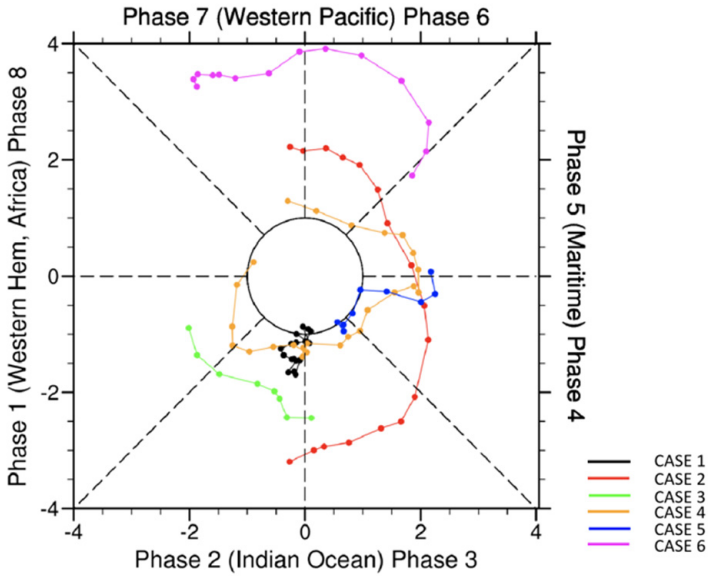

Figure 2. MJO phase and amplitude during the 6 CPEs.

2.3. Method

After eliminating wave numbers 1 to 3 and synoptic scale perturbations from 1979 to 2019, the average of the individual power spectra analyses of 40 winters T_{mins} in southern China was calculated to find the main oscillation periods, followed by Lancozs band-pass filters to analyze the intraseasonal variation of physical quantities.

A thermodynamic equation was used to investigate the contribution of different physical processes to the cooling process during the cold events. The equation can be written as follows:

$$\frac{\partial T}{\partial t} = -\left(u\frac{\partial T}{\partial x} + v\frac{\partial T}{\partial y}\right) + \omega(\gamma_d - \gamma) + \frac{1}{C_P}\dot{Q} \tag{1}$$

where γ_d is the dry adiabatic lapse rate, γ is the temperature lapse rate, C_P is the heat capacity at constant pressure, and $\dot{Q}$ is the diabatic heating. In Equation (1), any of the variables can be decomposed into the following components:

$$A = \overline{A} + A' + A'' + A^* \tag{2}$$

where $\overline{A}$ denotes the background field (>60 d), A' denotes the LF component (10–30-d), A'' denotes the LF component (30–60-d), and A^* denotes the synoptic-scale component (<10-d).

To study the propagation characteristics of the Rossby wave train, the wave activity flux (WAF) was calculated [41]. The WAF equation is as follows:

$$W = \frac{1}{2|\overline{U}|}\begin{pmatrix} \overline{u}\left(\psi'^2 - \psi'_x\psi'_{xx}\right) + \overline{v}\left(\psi'_x\psi'_y - \psi'\psi'_{xy}\right) \\ \overline{u}\left(\psi'_x\psi'_y - \psi'\psi'_{xy}\right) + \overline{v}\left(\psi'^2_y - \psi'\psi'_{yy}\right) \end{pmatrix} \tag{3}$$

where $|\overline{U}| = \sqrt{\overline{u}^2 + \overline{v}^2}$, ψ' represents the disturbance stream functions, and $\overline{u}$ and $\overline{v}$ are the 200-hPa winter mean latitudinal and meridional winds, respectively.

3. Intraseasonal Features of Temperature and Precipitation of CPEs in Southern China during Winter

3.1. Intraseasonal Features of Temperature

Figure 3 gives the mean power spectra of the T_{min} ISO component by calculating the average of the individual power spectra for each of the 40 winter seasons (1979–2019) in southern China. It can be inferred that there are two significant peaks at around 22 d and 40 d, and the analysis passes the 95% red noise test. This indicates that there is a clear intraseasonal oscillation cycle of 10–60-d for the winter T_{min} in southern China. Interestingly, there is a dip between the two peaks at around 28 d. In order to discuss the influence of the ISO over the mid-high-latitude and low-latitude MJO convective on the CPEs [25,42], the 10–60-d dominant periodicities are divided into 10–30-d and 30–60-d, which is beneficial for subsequent discussion. Many studies also discuss these two scales [43–45].

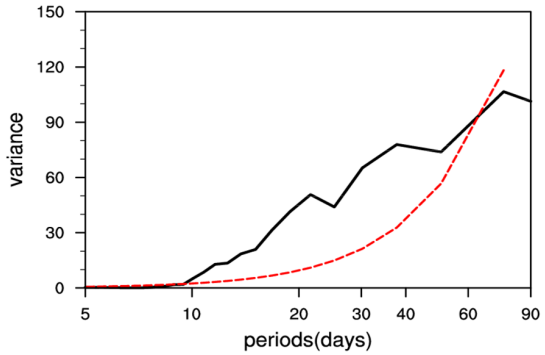

Figure 3. Winter mean power spectra of daily T_{min} in the southern region (20°–30° N, 105°–122.5° E) during 1979–2019. (The red line represents the 95% significant level of red noise spectrum).

Figure 4a depicts the spatial distribution of the contribution of 10–30-d LF T_{min} to the variance of winter T_{min}. It can be seen that there are apparent geographical differences across the country, progressively increasing from north to south, with the variance contribution of the LF temperature in the northern region being approximately 15%, over 25% in the southeast region, and even reaching over 30% in southern China. The variance contribution of LF components from 30 to 60 d accounts for a smaller percentage of the variance overall, and the large-value areas are predominantly concentrated in southern China, northern Xinjiang, and northwest Inner Mongolia of China (Figure 4b). This indicates that the LF variation in T_{min} is an important component of winter temperature in southern China compared to the western and northern regions, and consequently it is viable to study the ISO of low temperature in southern China.

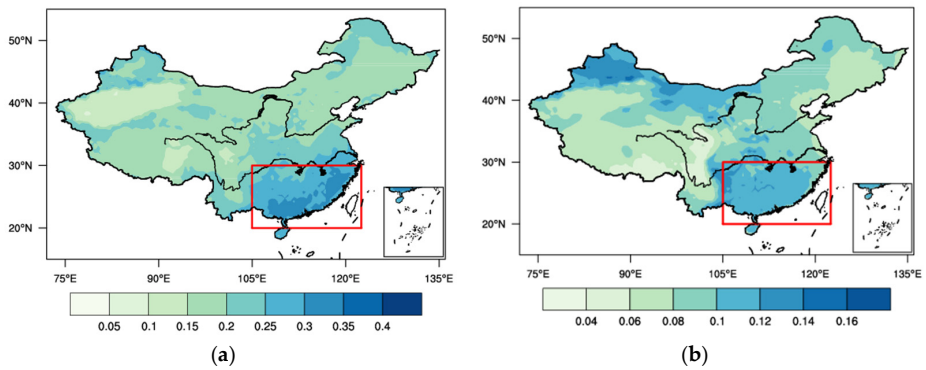

Figure 4. Ratio of 10–30-d filtered T_{min} variance (**a**) and 30–60-d filtered T_{min} variance (**b**) to 1979–2019 mean winter T_{min} variance spatial distribution. (The red box shows the southern region (20°–30° N, 105°–122.5° E).

3.2. LF Temperature and Precipitation Characteristics during CPEs in the Context of Strong MJO

Based on the definitions in Section 2, six CPEs influenced by strong MJO during the 40 winters from 1979 to 2019 were selected. Figure 5 shows the cold days and standardized 10–30-d/30–60-d filtered temperatures averaged over southern China during the six CPEs. It was revealed that the superimposition of the 10–30-d and 30–60-d periods in phase was largely responsible for the cooling process. After removing the annual cycle and filtering the synoptic scale perturbations, a complete fluctuation was defined as a wave from one peak to the next, with the temperature reaching a minimum value as the fifth phase, the previous peak as the first phase, the third and seventh phases as the positive and negative phase transitions, and the second (sixth) and fourth (eighth) phases as the temperature drop (rise) phase. The above definitions were used to make specific phase divisions for the six cold events, as shown in Figure 5 for one of the winter 2017 events. The following parts will focus on the effect of intraseasonal oscillations on these six events by phase synthesis.

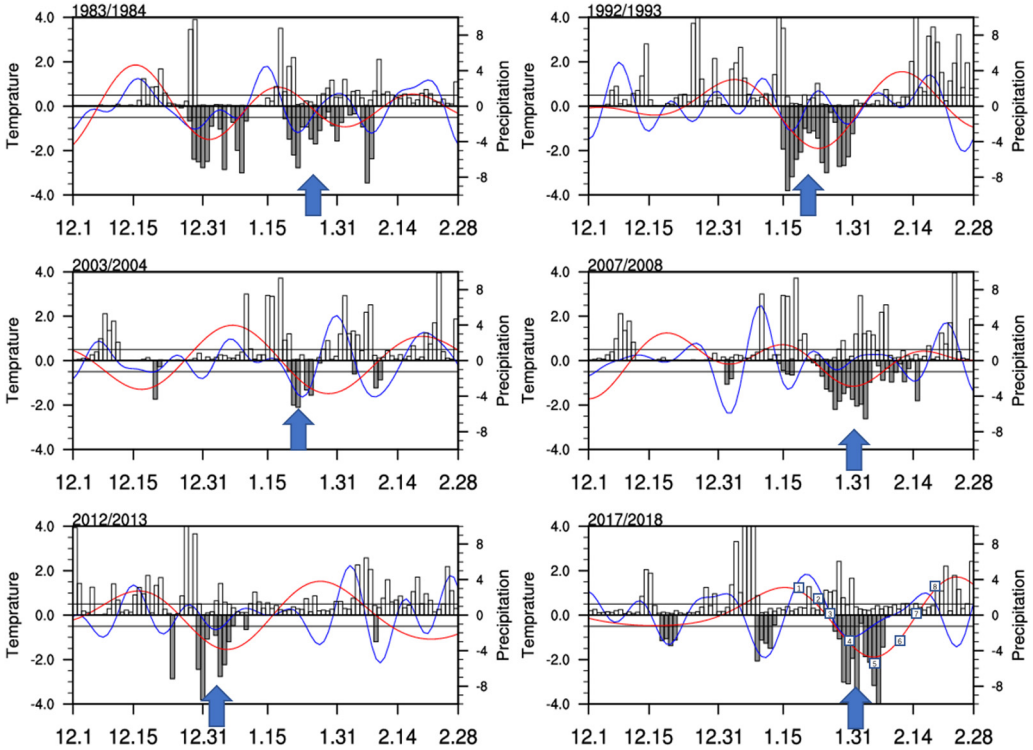

Figure 5. Time series of T_{min} minus thresholds corresponding (black bars) to extreme low-temperature days in southern China for 6 CPEs with filtered series from 10 to 30 d (blue line) and 30 to 60 d (red line) (left *y*-axis, unit: °C); white bars: precipitation (right *y*-axis, unit: mm/day); black line: ±0.5 standard deviation; blue arrows: CPEs; numbers 1–8: different phases of intraseasonal oscillations in Figure of 2017/2018 CPE.

What is noteworthy is that the six southern cold events analyzed were accompanied by precipitation during their cooling processes. Therefore, the precipitation during the six cold events will first be investigated. The 10–30-d filtered precipitation was synthesized according to the phase of temperature (Figure 6a). It can be seen that there are apparent negative precipitation anomalies over southern China at the first and second phases, while there are a few positive precipitation anomalies in the middle–lower reaches of Yangtze River. By analyzing the LF water vapor flux and temperature field at the lower level (850 hPa) (Figure 6b), there was observed a branch of northeast LF water vapor flux to the north of Yangtze River and a southwestward LF water vapor flux from the Bay of Bengal towards the south of China, which converge in the middle–lower reaches of the Yangtze River. In addition, abundant water vapor also comes from the South China Sea and the Northwest Pacific to the south of China. Although the water vapor conditions over

southern China are better, the lack of cold air intrusion from the north puts most of China in a positive temperature anomaly, which is not conducive to the production of rain and snow, and therefore there is an LF precipitation negative anomaly over a large area in phases 1–2. From the third phase onwards, the water vapor flux convergence zone gradually shifts southwards, accompanied by a large amount of cold air moving southwards, which meets both the convergence of cold and warm air and robust moisture conditions. After the fifth phase, precipitation moves eastward and weakens anomalously towards southern China as the cold advection gradually transports and weakens towards the coast.

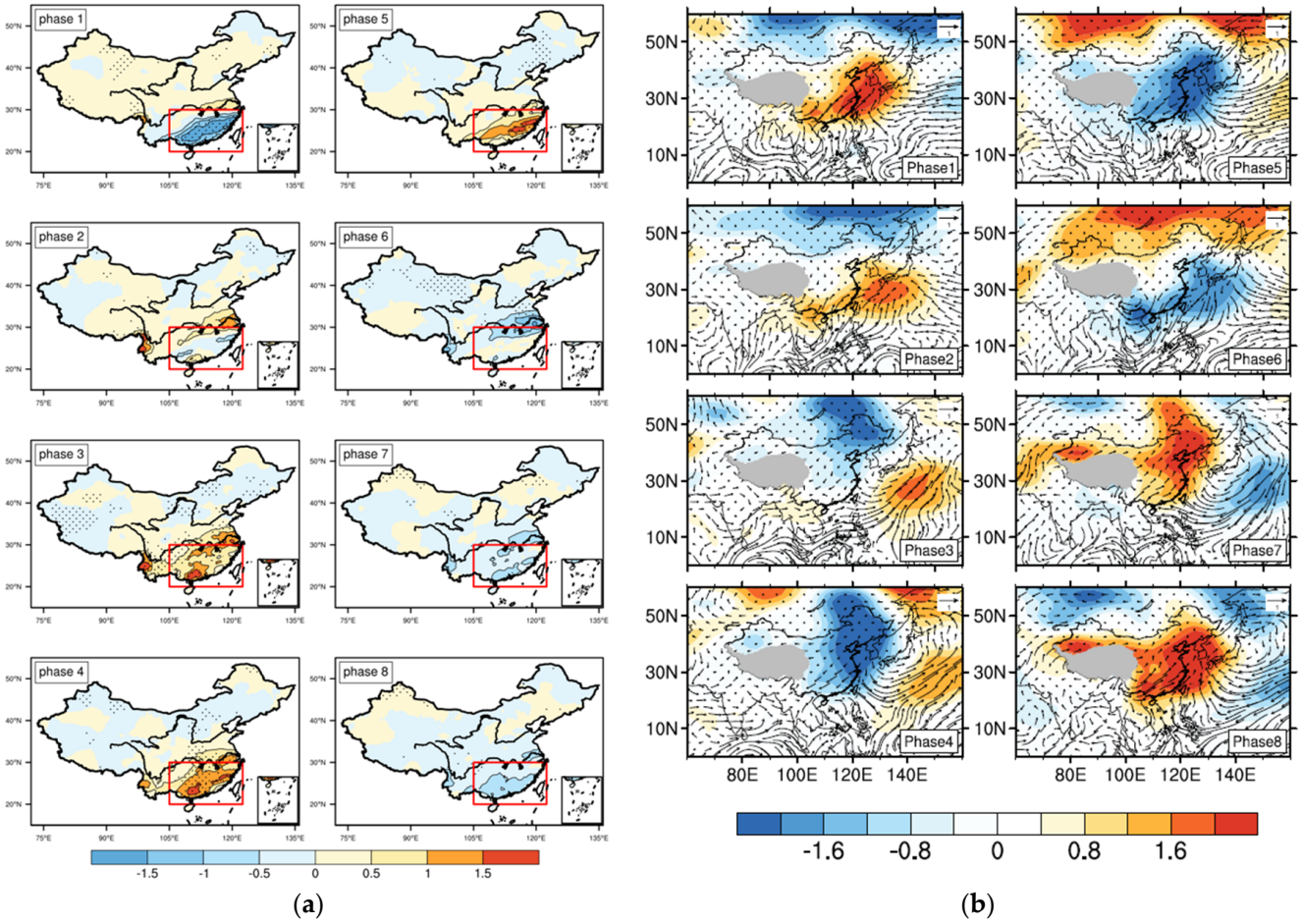

(**a**) (**b**)

Figure 6. The 10–30-d filtered (**a**) precipitation field (units: mm/day) and (**b**) 850-hPa temperature field (shading, unit: °C) and water vapor flux (vector, unit: $g \cdot cm^{-1} \cdot hPa^{-1} \cdot s^{-1}$) phase synthesis. (Dotted areas are where precipitation passed 95% significance test; grey area indicates the Tibetan Plateau).

The 30–60-d filtered LF precipitation evolution is similar to that of the 10–30-d period (figure omitted), and there is a better correspondence between the movement of the rainbands from the middle–lower reaches of the Yangtze River to the South China coast and the southward path of the cold air.

4. Characteristics and Evolution of Intraseasonal Circulation during CPEs in the Context of a Strong MJO

In the previous section, we revealed the intraseasonal characteristics of LF temperature and precipitation during the CPEs. What causes the evolution feature? Here, we intend to address the intraseasonal circulation during the CPEs. The low-level (925-hPa) temperature and wind fields were filtered for 10–30-d and 30–60-d to extract the intraseasonal signal. As shown in Figure 7, a strong LF anticyclone is present at the Ural Mountains and their vicinity in phase 1, while there is a weaker LF cyclone to the northwest of Lake Baikal and a strong

LF anticyclone over Japan. At this time, the East Asian winter monsoon is suppressed in the southern part of the country due to the southerly winds, accompanied by strong LF positive temperature anomalies; thus, the temperature is in a rising state. From the second phase onwards, the anticyclone over the Ural Mountains strengthens, moves eastwards, and is maintained to the west of Lake Baikal. The LF cyclone gradually moves eastwards to the Sea of Japan. In the fifth phase, the LF cyclone develops rapidly and deepens over the Sea of Japan, and the southern region is behind the LF cyclone. The northerly winds strengthen; therefore, the LF temperature anomaly over the southern region gradually changes from positive to negative. After the sixth phase, the cyclone moves markedly eastwards and weakens; the anticyclone anomaly moves further eastwards to the northwest Pacific, and a new cyclone gradually moves eastwards from eastern Europe to China. The combined effect of the cyclone and anticyclone causes southerly anomalies to prevail over eastern China, returning most of China to a warm anomaly.

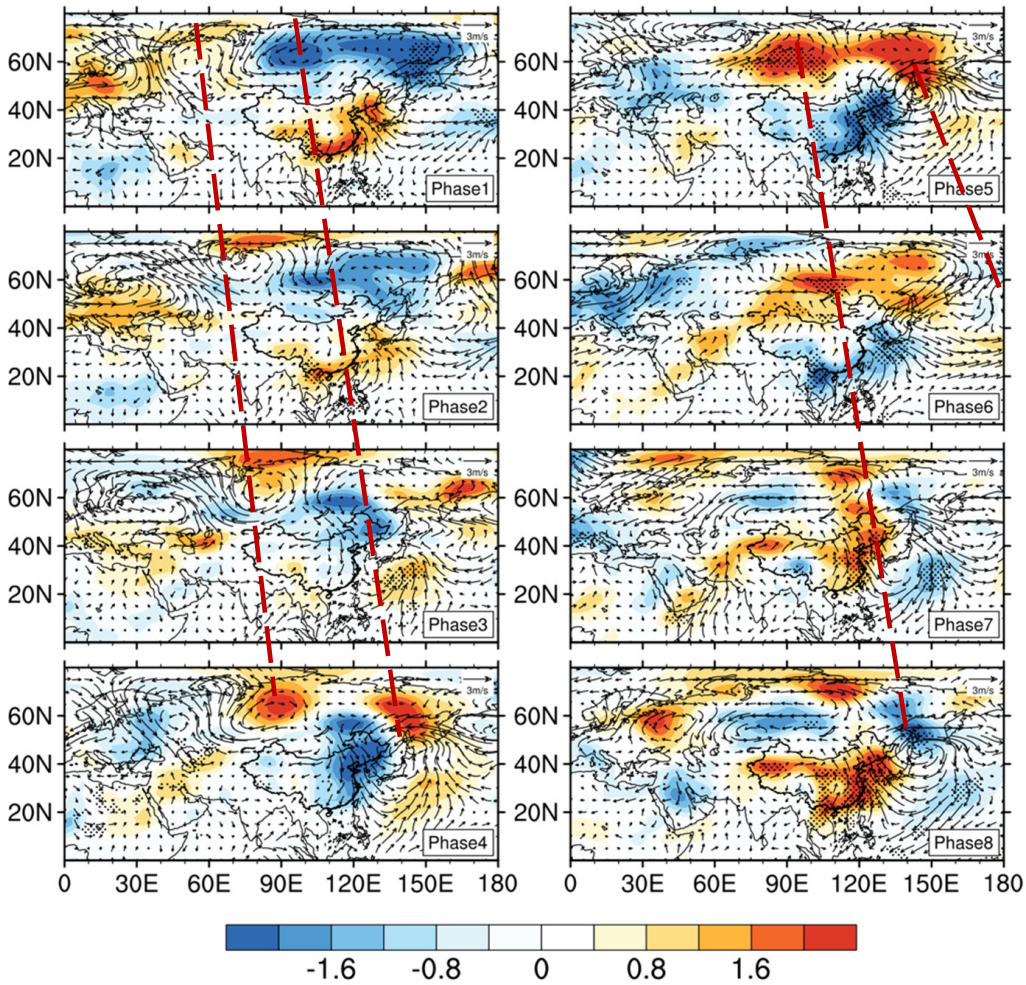

Figure 7. Temporal evolution of 10–30-d filtered 925-hPa temperature (shading, unit: °C) and wind (vector, unit: m·s^{-1}). (Dotted areas are where temperature passed 95% significance test; the red line is the cyclone and anticyclone).

The 925-hPa LF temperature and wind composite fields on the 30–60-d scale are comparable to those of the 10–30-d scale (figure omitted). The difference is that the anticyclone in the Siberian region is considerably stronger, and the range of its influence extends farther. The LF northeasterly winds at the front of the Siberian anticyclone intensify and guide the polar cold air to invade China continuously. At the end of the cold events, the anticyclone is replaced by an LF cyclone, which guides LF southwesterly winds to warm up southern China.

The above analysis suggests that cold advection is likely to be a significant factor in the occurrence of cold events. A diagnostic of the CPEs was therefore carried out by using the thermodynamic equation to explore the role of the temperature advection. Figure 8a shows that from the second phase onwards the term of temperature advection changes from positive to negative and gradually enhances, which is beneficial to the cooling process. In the early stages of the cooling, the term of negative adiabatic heating results from the adiabatic cooling of the ascending motion. The nonadiabatic heating is positive, reflecting that the intersection of cold and warm air over southern China leads to precipitation, which releases latent heat of condensation and weakens the cooling process. When the temperature drops to the minimum, the adiabatic heating term changes from a negative to a positive value, indicating that the ascending motion changes to a descending motion, which is not conducive to the cooling process. During the warming phase, a predominantly warm advection leads to an increase in temperature and the end of the low-temperature process. The 30–60-d filter gives similar results to the 10–30-d filter, but the values of the temperature advection and nonadiabatic changes are greater in the precooling phase (Figure 8b).

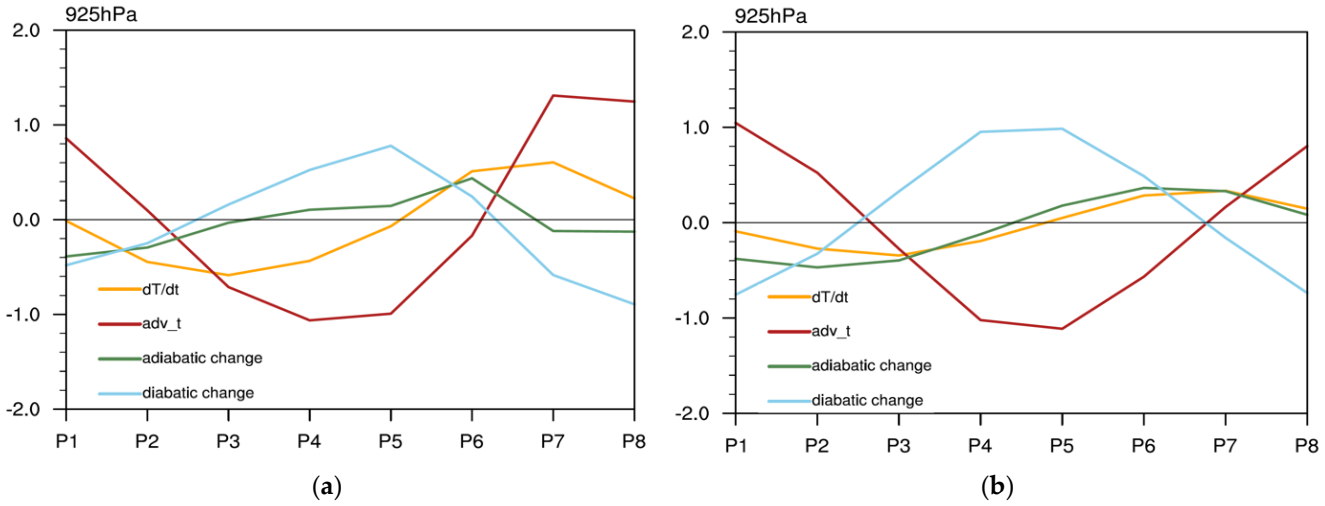

Figure 8. Thermodynamic equation budget (units: K d^{-1}) for the (**a**) 10–30-d and (**b**) 30–60-d filters at 925-hPa in southern China (20°–30° N, 105°–122.5° E).

Figure 9 gives the composition of the 10–30-d filtered geopotential height at the 500-hPa level and sea-level pressure (SLP) field accompanied with a barotropic '-+-'wave train over high latitudes, while the LF system is baroclinic at mid-latitudes. In the first phase, there is a positive SLP anomaly in the Ural Mountains and a strong negative anomaly in the Siberian Plateau. The positive anomaly then steadily moves southeastward to the west of Lake Baikal, where it strengthens and maintains, then merges with the positive anomaly coming from the northeast Pacific, resulting in a positive anomaly with large extension and intensity. This shows that the Siberian high tends to intensify in the early stage of the cold event, in favor of the cold air from the polar regions accumulating in Mongolia. In the LF 500-hPa potential height field, the gradual eastward shift of the Ural Mountains blocking high merges with the westward shift of the Okhotsk Sea blocking high in phase 3 and then is stagnant in the high latitudes. In phase 5, due to the compression and

merging of the two LF blocking high systems mentioned above, the negative anomaly of the LF northeastern cold vortex originally located in Siberia contracts southward over the Sea of Japan; thus, the anomalous northerly between the cold vortex and the blocking high steering the cold air from the high latitudes is the predominant factor in cold events. With the eastward diminishing and shifting of the system, the cooling process will gradually end.

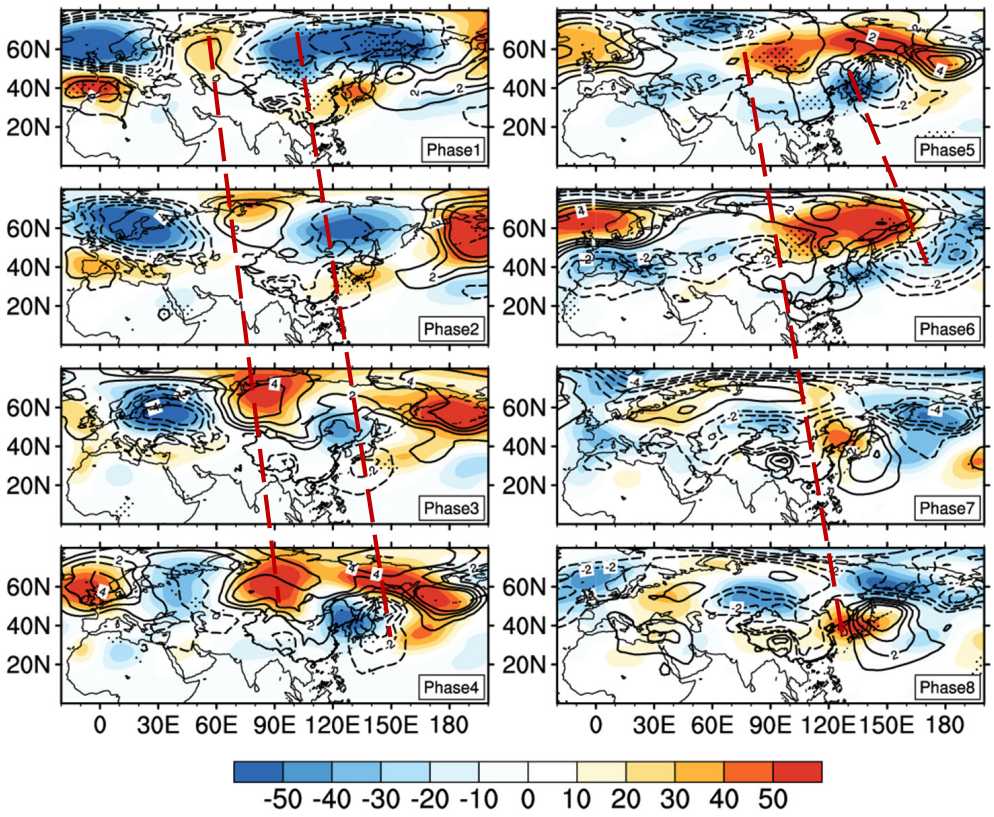

Figure 9. Temporal evolution of 10–30-d filtered 500-hPa geopotential height (shading, unit: gpm) and sea-level pressure (contours, unit: hPa) during six cold precipitation events. (Dotted areas are where height passed 95% significance test; the red line is the wave train shift).

The 30–60-d filtered 500-hPa geopotential height field and SLP field are similar to those of the 10–30-d filter (Figure 10); both show features of moving southeastward, a strengthening of the Asian cold high, and then constantly merging with the westward positive anomaly near the Sea of Okhotsk. The strengthening and spreading southward of the LF Siberian high is more robust with its south boundary reaching South China. The 30–60-d filtered 500-hPa height field is characterized by positive and negative meridional waves in Eurasia, while the two LF blocking highs merge with and form a stronger and more extensive center, which is maintained for a longer period of time. All of the above characterize a more intense activity of cold air in southern China on the 30–60-d scale.

From the analysis of the LF circulation during the CPEs, it was learned that the contraction of the two LF blocking highs in the mid-high latitudes of the Ural Mountains and the Sea of Okhotsk at the 500-hPa level causing the contraction of the LF northeastern cold vortex to be reinforced, the northerly wind between the cyclone and anticyclone at 925 hPa facilitating the southward movement of cold air, and the southward movement of the LF Siberian cold high in the SLP field were important reasons for the formation of the cold events.

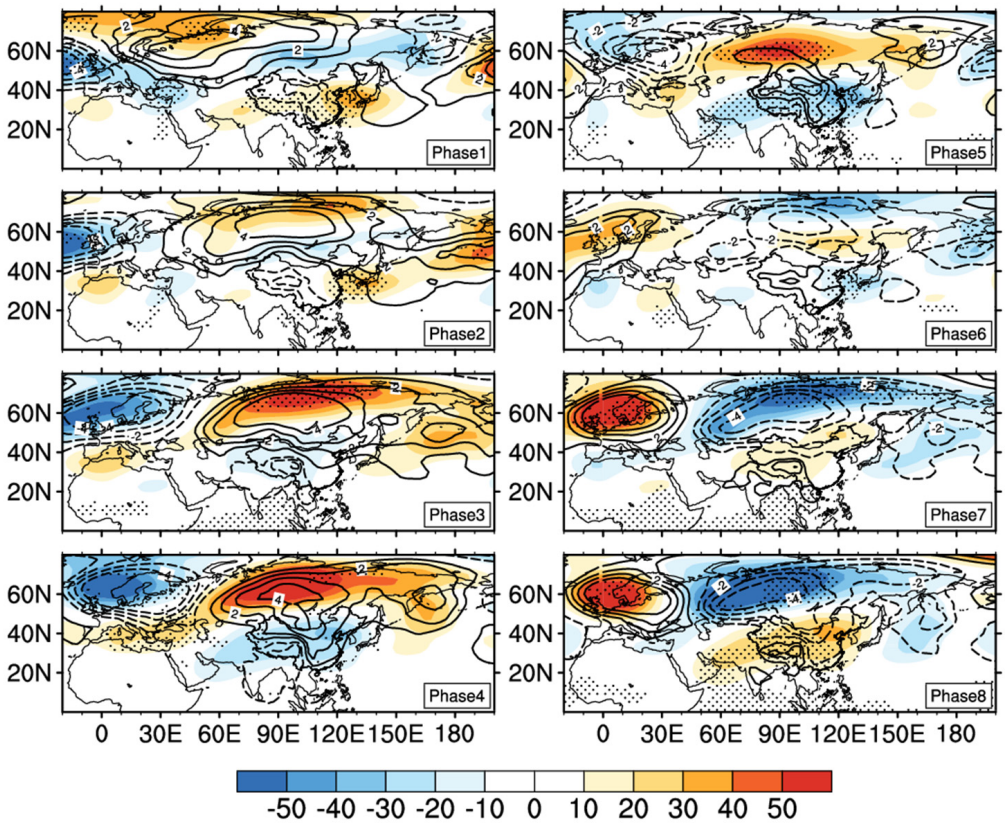

Figure 10. Temporal evolution of 30–60-d filtered 500-hPa geopotential height (shading, unit: gpm) and sea-level pressure (contours, unit: hPa) during six cold precipitation events. (Dotted areas are height passing 95% significance test).

5. The Impact of the MJO on CPEs

In order to investigate the link between the MJO and CPEs, a correlation analysis was performed using the RMM index and the synthetic field of the fifth phase (P5) with the most significant low-temperature feature after the 30–60-d filter. According to Jin and Hoskins [46], the Rossby waves for a given tropical heating response is adequately established within 15 d. Hence, the time-lead correlation analysis was performed using 0, 5, 10, and 15 d of the leading P5 of the 200-hPa geopotential height field. It can be seen (Figure 11) that at the same time (lag0) there are two positive correlations anchoring over the west of Lake Baikal and the Sea of Okhotsk which are weak and progressively become stronger as the leading time increased. Accordingly, the MJO had some effect on the LF systems in the mid-high latitudes, and then induced the persistent low temperature over southern China.

The 200-hPa wave activity flux and geopotential height field anomalies were synthesized for the P5 at each oscillation period. From the results of the 10–30-d filtering (Figure 12a), the 200-hPa LF height field appears as a large positive anomaly formed by the merger of the LF high over the Siberian region and the northwest Pacific and a negative anomaly center in the northeast of China, which is similar to the distribution at 500 hPa with a barotropic structure. The Rossby waves in the high latitudes originate from the Nordic region, and from this center they propagate eastwards along the positive anomaly center in Siberia and gradually start to have a southward dispersive component on the east side of the Ural Mountains, passing through Mongolia and propagating to the northeast of China, making the anomalous circulation reinforced and retained. The 30–60-d filtered LF height field (Figure 12b) illustrates that highs exist in the Black Sea, Central Siberia, the northwest Pacific, and the northern Bay of Bengal, and that they "surround" the negative height anomaly in the northeastern part of China. The wave activity fluxes show that, in addition to a wave flux from high latitudes, there is also a northeastward wave flux

near the Bay of Bengal at low latitudes, and the two converge at the negative anomaly in eastern China.

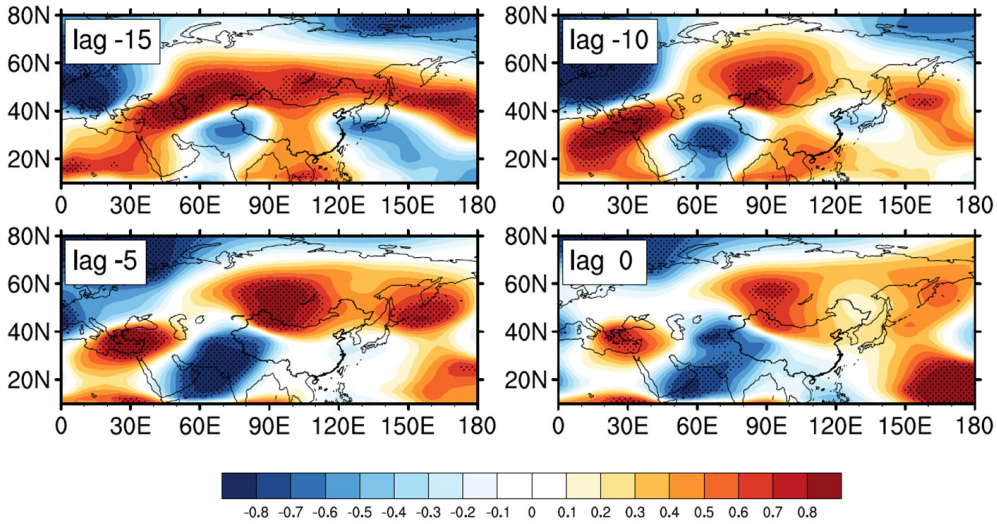

Figure 11. RMM index and the fifth-phase 200-hPa height field lead correlation. (Lag-n denotes leading of phase 5 of the 30–60-d filter for n days. Dotted areas indicate correlations passing the 95% significance test).

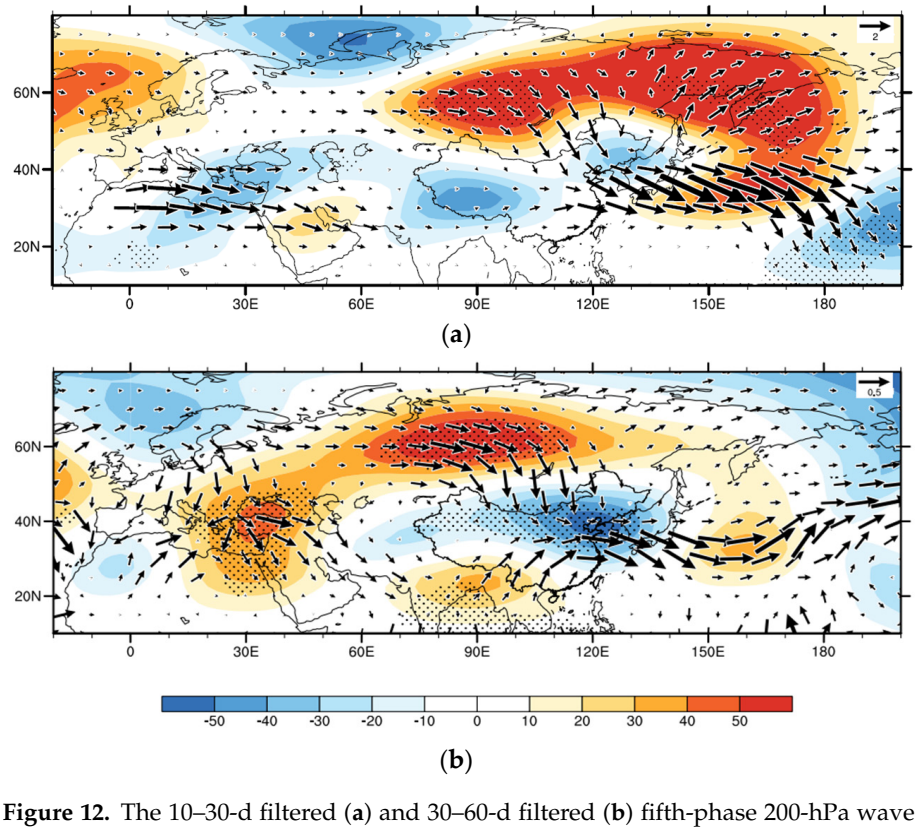

Figure 12. The 10–30-d filtered (**a**) and 30–60-d filtered (**b**) fifth-phase 200-hPa wave activity flux (vector arrow, unit: $m^2 \cdot s^{-2}$) and height fields (shading, unit: hPa). (Dotted areas are height passing 95% significance test).

To further demonstrate whether the above 30–60-d low-latitude signal is directly related to the MJO, the anomaly fields of the 30–60-d filter were synthesized in the low-temperature phase (Figure 13). The results show that in the cooling phase the negative LF outgoing longwave radiation (OLR) anomaly in the Indian Ocean gradually expands in

extent, strengthens gradually, and moves eastward, while convective activity in the South China Sea and the western Pacific is weaker, indicating that the MJO convective center is exceptionally active over the Indian Ocean at this time. It has been pointed out [47] that when the MJO convective center is active over the Indian Ocean the probability of a sustained low-temperature event is comparatively higher in most parts of China, which is consistent with the results of this paper. It is worth noting that during this phase there is also a strong east–west negative anomaly zone from the eastern part of the mainland of China to southern Japan. In the late warming phase, the OLR anomaly over the Indian Ocean region gradually turns into a positive anomaly, indicating that the suppression of the tropical MJO convective activity at this time may reduce the occurrence of low-temperature events. The 500-hPa vertical velocity field is also well-matched with the center of the MJO convective activity, with strong anomalous ascending motion in the active convective region over the Indian Ocean and southeastern China during the cooling phase, and anomalous descending motion in the western Pacific. We notice that the OLR anomaly over southeastern China corresponds well to the precipitation regions (Figure 6a). Liu and Yang [48] found that the probability of precipitation in southeastern China in the winter is significantly increased when the center of the MJO convective activity is located in the Indian Ocean region, which is consistent with the results of this paper.

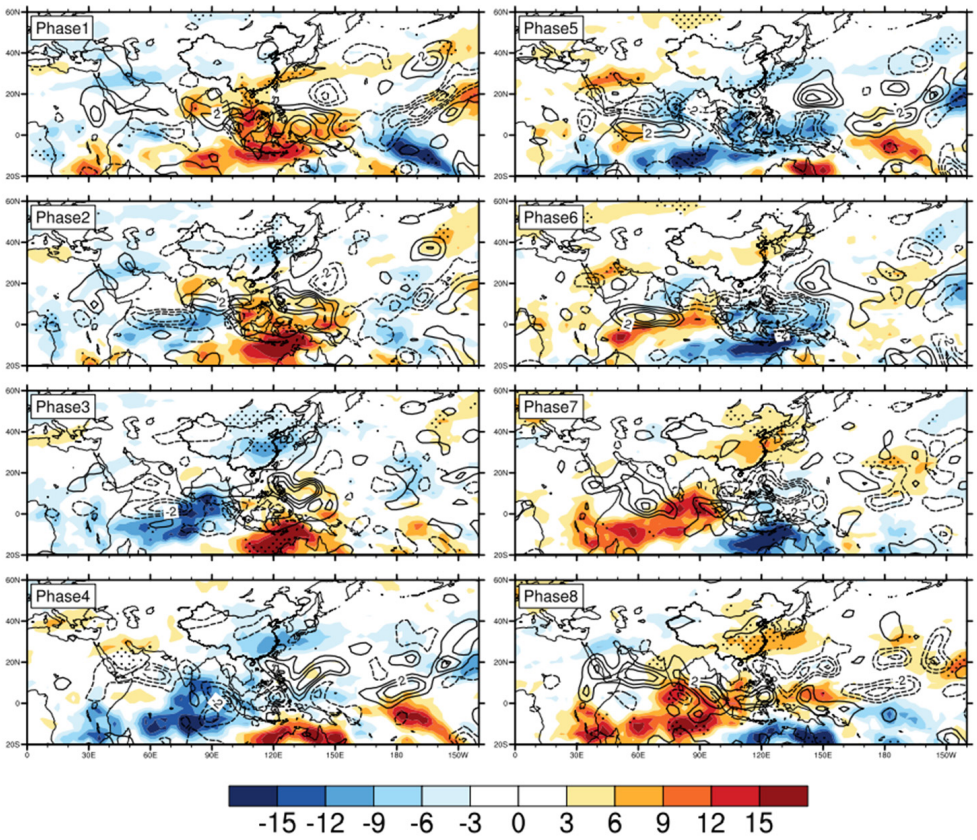

Figure 13. The 30–60-d filtered OLR anomaly field (shading, unit: $W \cdot m^{-2}$) and 500-hPa omega anomaly field (contours, unit: $hPa \cdot s^{-1}$). (Dotted areas are OLR passing 95% significance test).

6. Conclusions and Discussion

6.1. Conclusions

This paper defines extreme low temperature thresholds based on daily T_{min} data in China and focuses on the intraseasonal oscillation of six cold precipitation events in winter in southern China under the influence of strong MJO. The main conclusions can be summarized as follows:

1. Winter temperatures in southern China are characterized by significant 10–30-d and 30–60-d ISOs, and CPEs in the context of a strong MJO all occur under the two intraseasonal scales in cooling phases. The invasion of cold air coupled with the availability of appropriate moisture conditions in southern China is more conducive to the occurrence of CPEs in winter.
2. A cyclone and anticyclone from the east of the Ural Mountains and the northwest of Lake Baikal gradually moves southeastward in the low troposphere. The LF blocking highs over the Ural Mountains and the North Pacific at 500-hPa merge to cause the LF cold vortex contract and move southward. The following anomalous northerly winds steer the cold air towards southern China. The diagnosis of the 925-hPa thermodynamic equation indicates that the dominant term in the cooling process is cold advection, while the adiabatic cooling accompanied with ascending motion is also beneficial to the cooling process.
3. The correlation analysis and 200-hPa wave activity flux show that the MJO and LF signal in the mid-high latitude are most significant on the leading 15 d. MJO will have some effect on the LF blocking highs and the cold vortex in the mid-high latitudes and then induces the CPEs over southern China. The joint effect of mid-high and low latitudes on the 30–60-d scale can have a significant impact on the cooling and precipitation processes of CPEs.

6.2. Discussion

A synthetic analysis of six CPEs in the context of a strong MJO reveals that the opposite movement of an LF blocking high to the east of the Ural Mountains and the North Pacific plays a crucial role in the CPEs; however, this feature is not present in all cold events. We found four CPEs under the influence of weak MJO in ten CPEs selected earlier. It is worth mentioning that the changes and intensities affecting the low-frequency system at mid-high latitudes in CPEs are also different under the different intensities of MJO. Consequently, further work should be performed to explore the extent to which MJO influences low temperatures and precipitation in the winter. According to recent views [49,50], surface air temperature (SAT) anomalies at mid-high latitudes are more influenced by changes in mid-high latitude systems, such as the Siberian high (SH) and the Arctic Oscillation (AO), so the influence of MJO can only be regarded as an additional factor with limited influence. Is it possible to classify CPEs in southern China using a cluster analysis method and separate the tropical MJO and mid-high-latitude ISO signals that affect the CPEs? In addition, due to the fewer event samples discussed in this paper, it is also possible to reduce the standard for defining CPEs before analyzing them. Then, with a larger number of samples, observing whether there is a regular pattern in the MJO phase during the CPEs will also deserve attention in future work.

Author Contributions: Conceptualization and methodology, Q.G.; data curation, Z.Z., S.C. and Y.Z.; writing—original draft preparation, Q.G. and Z.Z.; writing—review and editing, Q.G. All authors have read and agreed to the published version of the manuscript.

Funding: This work was supported by the National Natural Science Foundation of China (42075032) and the National Key Research and Development Program of China (2018YFC1505804).

Institutional Review Board Statement: Not applicable.

Informed Consent Statement: Not applicable.

Data Availability Statement: Thanks to the China Meteorological Data Network, National Oceanic and Atmospheric Administration (NOAA), and National Centers for Environment Prediction/Department of Energy (NCEP/DOE) for providing datasets.

Conflicts of Interest: The authors declare no conflict of interest.

References

1. Cohen, J.; Screen, J.A.; Furtado, J.C.; Barlow, M.; Whittleston, D.; Coumou, D.; Francis, J.; Dethloff, K.; Entekhabi, D.; Overland, J.; et al. Recent Arctic amplification and extreme mid-latitude weather. *Nat. Geosci.* **2014**, *7*, 627–637. [CrossRef]
2. Zhu, W.; Li, Q.; Wang, Z.; Shen, X. Climatological variability of cold air processes over China in recent 60 years. *Meteorol. Mon.* **2022**, *48*, 1–13. (In Chinese)
3. Kug, J.; Jeong, J.; Jang, Y. Two distinct influences of Arctic warming on cold winters over North America and East Asia. *Nat. Geosci.* **2015**, *8*, 759–762. [CrossRef]
4. Song, L.; Wu, R. Combined effects of the MJO and the Arctic Oscillation on the intra-seasonal Eastern China winter temperature variations. *J. Clim.* **2019**, *32*, 2231–2295. [CrossRef]
5. Han, R.; Shi, L.; Yuan, Y. Analysis on the causes of cold and warm transition in China during the winter of 2020/2021. *Meteorol. Mon.* **2021**, *47*, 880–892.
6. Jiang, Z.; Long, F. Analysis of effect on agriculture in Guilin by chilling icy rain and snow freezing disasters. *J. Meteorol. Res. Appl.* **2008**, *29*, 50–51. (In Chinese)
7. Yang, J.; Ren, C.; Jiang, Z. Characteristics of extreme temperature event and its response to regional warming in Northwest China in past 45 years. *Chin. Geogr. Sci.* **2008**, *18*, 70–76. [CrossRef]
8. Ma, N.; Li, Y.; Ju, J. Intra-seasonal oscillation characteristics of extreme cold-snowy and freezing rainy weather in Southern China in early2008. *Plateau Meteorol.* **2011**, *30*, 318–327. (In Chinese)
9. Bueh, C.; Peng, J.; Xie, Z.; Ji, L. Recent progresses on the studies of wintertime extensive and persistent extreme cold events in China and large-scale tilted ridges and troughs over the Eurasian Continent. *Chin. J. Atmos. Sci.* **2018**, *42*, 656–676. (In Chinese)
10. Qian, W.; Zhang, Z. Precursors to predict low-temperature freezing-rain events in southern China. *Chin. J. Geophys.* **2012**, *55*, 1501–1512. (In Chinese)
11. Madden, R.A.; Julian, P.R. Detection of a 40-50day oscillation in the zonal wind in the tropical Pacific. *J. Atmos. Sci.* **1971**, *28*, 702–708. [CrossRef]
12. Madden, R.A.; Julian, P.R. Description of global scale circulation cells in the tropics with 40-50day period. *J. Atmos. Sci.* **1972**, *29*, 1109–1123. [CrossRef]
13. Anderson, J.R.; Rosen, R.D. The latitude-height structure of 40-50day variations in atmospheric angular momentum. *J. Atmos. Sci.* **1983**, *40*, 1584–1591. [CrossRef]
14. Li, C. Global characteristics of 30-60-day atmospheric oscillation. *Chin. J. Atmos. Sci.* **1991**, *15*, 66–76. (In Chinese)
15. Li, C.; Long, Z.; Mu, M. Atmospheric intra-seasonal oscillations and its important effect. *Chin. J. Atmos. Sci.* **2003**, *27*, 518–535. (In Chinese)
16. Qiu, M.; Lu, W.; Wang, S. ENSO episodes and low-frequency oscillations in the extra-tropical latitude of the northern hemisphere. *J. Trop. Meteorol.* **2006**, *22*, 454–460. (In Chinese)
17. Tim, L. Recent Advance in Understanding the Dynamics of the Madden-Julian Oscillation. *J. Meteorol. Res.* **2014**, *28*, 1–33.
18. Li, C.; Liu, Y.; Li, X. Impact of the 10-30-day oscillation intensity over the tropical northwest Pacific on the South China Sea summer monsoon. *J. Appl. Meteorol. Sci.* **2016**, *27*, 293–302. (In Chinese)
19. Li, T.; Ling, J.; Hsu, P. Madden–Julian Oscillation: Its discovery, dynamics, and impact on East Asia. *J. Meteorol. Res.* **2020**, *34*, 20–42. [CrossRef]
20. Wang, M.; Duan, A. Quasi-Biweekly Oscillation over the Tibetan Plateau and its link with the Asian Summer Monsoon. *J. Clim.* **2015**, *28*, 4921–4940. [CrossRef]
21. Jiang, X.; Li, T. Reinitiation of the boreal summer intra-seasonal oscillation in the tropical Indian Ocean. *J. Clim.* **2005**, *18*, 3777–3795. [CrossRef]
22. Yang, S.; Wu, B.; Zhang, R. Propagation of low-frequency oscillation over Eurasian mid-high latitude in winter and its association with the Eurasian teleconnection pattern. Chin. *J. Atmos. Sci.* **2014**, *38*, 121–132. (In Chinese)
23. Zhou, S.; Miller, A.J. The interaction of the Madden—Julian oscillation and the Arctic Oscillation. *J. Clim.* **2005**, *18*, 143–159. [CrossRef]
24. Watanabe, T.; Yamazaki, K. The upper-level circulation anomaly over central Asia and its relationship to the Asian monsoon and mid-latitude wave train in early summer. *Clim. Dyn.* **2014**, *42*, 2477–2489.
25. Matthews, A.J.; Hoskins, B.J.; Masutani, M. The global response to tropical heating in the Madden–Julian oscillation during the northern winter. Quart. *J. R. Meteorol. Soc.* **2004**, *130*, 1991–2011. [CrossRef]
26. Ren, J.; Zheng, J.; Xu, Y.; Tao, Y.; Zhang, W.; Ju, J. The intra-seasonal oscillation of Siberian High influenced on the winter temperature of Yunnan in 2007. *J. Yunnan Univ.* **2015**, *37*, 386–398. (In Chinese)
27. Li, Y.; Wang, J.; Wang, S. The integrated circulation anomalies of polar vortex, blocking and the Siberian high over the extreme low-temperature events. *J. Lanzhou Univ. (Nat. Sci.)* **2019**, *55*, 51–63. (In Chinese)
28. Tan, G.; Zhang, W. The 10–30 d low-frequency variation of winter surface air temperature in China and its relationship with Ural Mountain circulation. *Trans. Atmos Sci.* **2018**, *41*, 502–512. (In Chinese)
29. Zhu, Y.; Jiang, J. The intra-seasonal characteristics of wintertime persistent cold anomaly in China and the role of low-frequency oscillations in the low latitude and midlatitude. *J. Trop. Meteorol.* **2013**, *29*, 649–655.
30. Miao, Q.; Gong, Y.; Deng, R. Impacts of the low-frequency oscillation over the extra-tropics of the Northern Hemisphere on the extreme low temperature event in Northeast China in the winter of 2012/2013. *Chin. J. Atmos. Sci.* **2016**, *40*, 817–830. (In Chinese)

31. Yu, W.; Gao, Q. Analysis and diagnosis of low-frequency characteristics in a low temperature event in southern China in the winter of 1996. *Chin. J. Atmos. Sci.* **2020**, *44*, 257–268. (In Chinese)
32. Jiang, Y.; Yao, S.; Wang, Y. Intra-seasonal oscillation characteristics of low temperature events in January 2016. *J. Meteorol. Sci.* **2019**, *39*, 42–49. (In Chinese)
33. Chen, X.; Ling, J.; Li, C.; Li, L.; Yang, M. Different impacts of Madden–Julian oscillation on winter rainfall over southern China. *J. Meteorol. Res.* **2021**, *35*, 271–281. [CrossRef]
34. Zhang, C. Madden–Julian oscillation: Bridging weather and climate. *Bull. Am. Meteorol. Soc.* **2013**, *94*, 1849–1870. [CrossRef]
35. Wu, J.; Yuan, Z.; Qian, Y. The role of intra-seasonal oscillation in the southern China snowstorms during January 2008. *J. Trop. Meteorol.* **2009**, *25*, 103–111. (In Chinese)
36. Jia, X.; Liang, X. Possible impacts of Madden–Julian Oscillation on the severe rain-snow weather in China during November 2009. *J. Trop. Meteorol.* **2013**, *19*, 233–241. (In Chinese)
37. Wu, J.; Gao, X. A gridded daily observation dataset over China region and comparison with the other datasets. *Chin. J. Geophys.* **2013**, *56*, 1102–1111. (In Chinese)
38. Liebmann, B.; Smith, C.A. Description of a complete (interpolated) outgoing long wave radiation dataset. *Bull. Am. Meteorol. Soc.* **1996**, *77*, 1275–1277.
39. Wheeler, M.C.; Hendon, H. An all-season real-time multivariate MJO index: Development of an index for monitoring and prediction. *Mon. Weather Rev.* **2004**, *132*, 1917–1932.
40. Peng, J.; Bueh, C. The definition and classification of extensive and persistent extreme cold events in China. Atmos. *Oceanic Sci. Lett.* **2011**, *4*, 281–286.
41. Takaya, K.; Nakamura, H. A formulation of a phase-independent wave-activity flux for stationary and migratory Quasi-geostrophic eddies on a zonally varying basic flow. *J. Atmos. Sci.* **2001**, *58*, 608–627. [CrossRef]
42. Kim, S.; Kug, J.; Seo, K. Impacts of MJO on the intra-seasonal temperature variation in East Asia. *J. Clim.* **2020**, *33*, 1–34. [CrossRef]
43. Yang, J.; Wang, B.; Bao, Q. Biweekly and 21–30-Day variations of the subtropical summer monsoon rainfall over the lower reach of the Yangtze River Basin. *J. Clim.* **2010**, *23*, 1146–1159. [CrossRef]
44. Sun, X.; Jiang, X.; Yang, X. Role of intra-seasonal oscillation in the persistent extreme precipitation over the Yangtze River Basin during June 1998. *J. Geophys. Res. Atmos.* **2016**, *121*, 10453–10469. [CrossRef]
45. Yang, J.; Wang, B. Anticorrelated intensity change of the quasi-biweekly and 30-50-day oscillations over the South China Sea. *Geophys. Res. Lett.* **2008**, *35*, 797–801. [CrossRef]
46. Jin, F.; Hoskins, B.J. The Direct Response to Tropical Heating in a Baroclinic Atmosphere. *J. Atmos. Sci.* **1995**, *52*, 307–319. [CrossRef]
47. Zhang, W.; Jiang, J. Influence of Madden–Julian Oscillation on winter persistent cold events in China. *Sci. Meteorol. Sin.* **2015**, *35*, 422–429. (In Chinese)
48. Liu, D.; Yang, X. Mechanism responsible for the impact of Madden–Julian Oscillation on the wintertime rain-fall over eastern China. *Sci. Meteorol. Sin.* **2010**, *30*, 684–693. (In Chinese)
49. Cui, J.; Yang, S.; Tim, L. Relationship between the Madden-Julian oscillation and high-latitude surface air temperature during boreal winter. *Meteorol. Mon.* **2021**, *47*, 49–59. (In Chinese)
50. Abdillah, M.R.; Kanno, Y.; Iwasaki, T. Cold surge pathways in East Asia and their tropical impacts. *J. Clim.* **2021**, *34*, 157–170. [CrossRef]